This article has been accepted for publication in a future issue of this journal, but has not been fully edited. Content may change prior to final publication. Citation information: DOI 10.1109/JLT.2015.2397191, Journal of Lightwave Technology

Fully-Switchable Multi-Wavelength Fiber Lasers Based on Random Distributed Feed-Back for Sensors Interrogation

Mikel Bravo, Veronica de Miguel, Amaia Ortigosa and Manuel Lopez-Amo, *Senior Member, IEEE.*

***Abstract*—. In this paper, the experimental study and characterization of a novel real-time switchable multi-wavelength fiber laser has been carried out. Two different gain materials, such as a 50 km SMF and a 2.5 km DCF fibers were characterized and compared, respectively. The MWFL can generate any wavelength combination with an emission lines distance of 50, 100 and 200 GHz fitting the ITU grid specifications. By using both Er-doped fiber and Raman amplification, a ~30 nm wide lasing window at the C band can be utilized to create up to 30 different lasing wavelengths into the ITU Grid, that can be switched automatically and in real-time when desired. Utilization of such a laser for versatile interrogation of different sensing networks is also shown.**

Index Terms*—. *Switchable multi-wavelength fiber laser, random distributed feed-back.

I. Introduction

Multi-wavelength fiber lasers (MWFL) have attracted much interest recently because of their potential applications in wavelength-division-multiplexing (WDM) communications, high-resolution spectroscopy and fiber optic sensing [1]. The possibility of reconfiguring the output spectrum of a source for sensing purposes is a field wherein other researches had focused his attention [2]. R. A. Perez-Herrera *et al.* proposed a switchable MWFL based on Erbium-doped fiber amplifier for FBG remote sensing [3].

Recently, several MWFLs have been demonstrated using random mirrors in combination with another kind of mirrors or filter structures, which usually act as wavelength selectors [4-10]. Random lasers based on Rayleigh scattering feedback and amplified through Raman´s effect have been the subject of intense theoretical and experimental study [11]. Random lasers are characterized by open-cavities or mirror-less-cavities which means that, unlike conventional fiber lasers, their principle of operation rely on distributed scattering events along the fiber cavity [12]. By using FBG sensors as wavelength selectors in combination with distributed mirrors, MWFL lasers for remote sensing have been proposed in [13]

This paper presents the characterization and the experimental demonstration of a fully-switchable MWFL assisted by a distributed mirror. This structure [7] was characterized in this paper for two kinds of fibers as Raman amplification media. And finally, it was used for the first time as a proof of concept for remote sensor multiplexing of different sensing technologies. In this demonstration, different sensing technologies and multiplexing topologies were sequentially interrogated. The laser enables simultaneous spatial and WDM multiplexing techniques for different sensors based on wavelength switching and sweeping [14].

Manuscript received September, 5, 2014. This work was supported by the Spanish Government projects TEC2010-20224-C02-01, TEC2013-47264-C2-2-R, INNOCAMPUS and by the European SUDOE-Interreg Project ECOAL-MGT, and FEDER funds.

M. Bravo, V. DeMiguel, A. Ortigosa and M. Lopez-Amo, are with Department of Electric and Electronic Engineering, Public University of Navarra, Campus Arrosadia S/N, 31006, Navarra, Spain. (e-mail: mikel.bravo@unavarra.es).

II. MWFL Experimental Characterization.

A fiber laser which utilizes a random mirror has been dynamically filtered by a mirror-filtering structure to achieve a switchable and reconfigurable fiber optic laser. The dynamical filtering is possible by using the Finisar WaveShaper 1000S. Here, two different active fibers as Raman amplification media are studied. The fibers used are a ~2.5 km long DCF (dispersion compensated fiber) and a 50 km SMF (single mode fiber).

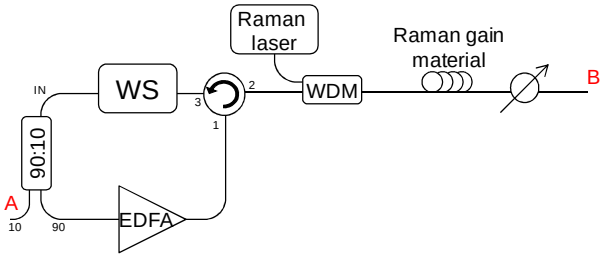

Fig. 1. Schematic representation of the setup for the switchable and reconfigurable multi-wavelength random fiber laser. WS: WaveShaper programmable filter

Figure 1 illustrates the schematic setup of the switchable and reconfigurable laser. The laser is based on a linear cavity formed of two mirrors. The first one (right side and labeled as Raman gain material), is a RDFB based mirror generated into, in one case, a ~2.5 km DCF reel [7] and in the other, a 50 km reel of SMF. The second mirror (left side) is formed of a loop mirror created by connecting the input/output ports of a circulator as shown in figure 1. This mirror has the role of

This article has been accepted for publication in a future issue of this journal, but has not been fully edited. Content may change prior to final publication. Citation information: DOI 10.1109/JLT.2015.2397191, Journal of Lightwave Technology

filtering the light into the cavity to select the spectrum profile of the switchable and reconfigurable multi-wavelength random laser. In order to perform this feature, the programmable tunable filter was used. On the other hand, an Erbium doped fiber amplifier (EDFA) was also used because the combination of the Erbium gain profile and the Raman´s one allows us to have a broad comb laser spectrum (up to ~30 nm) and up to 10 dBm output powers. The operation mode of the system was presented in [7].

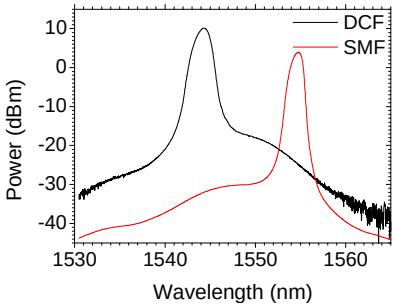

Fig. 2. Both, DCF and SMF laser spectrum when the WaveShaper filter is off.

Following, the characterizations of the SMF based MWFL are presented in comparison of the DCF one. The lasing performance, the maximum number of emission lines, the lines' widths and the lines' separation were studied. Although this configuration is able to create any multi-wavelength laser configuration, the ITU grid specifications were taken as a reference for this study. 200, 100 and 50 GHz separation distances were tested in the proposed setup. Thus, a custom program was developed to control the programmable filter. This software fully meets the desired requirements by selecting the suitable comb filter configuration. Moreover, an equalization feature and other facilities for the studies presented were also developed.

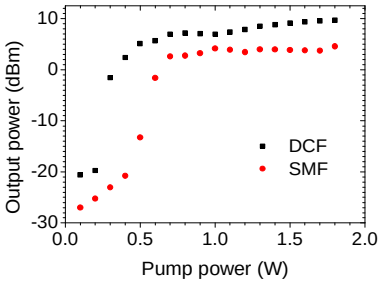

Fig. 3. Laser power evolution versus pump power obtained for DCF (a) and SMF (b) lasers

First of all, figure 2 shows the laser spectrum of the two systems under study when the WhaveShaper filter is off. As it is aforementioned, two different lasers were developed using two different fiber spools. The first one is the DFC one with a length of 2.5 km, a -343 ps/(nm*km) first order dispersion coefficient at 1545 nm and an effective area of 21 μm^2. The other one is a standard single-mode fiber reel of 50 km. The main difference between both lasers is the broader spectrum shape of the SMF scheme although the maximum power achieved is lower than in the DCF one. Thus, it is expected to reach a broader comb laser performance with the SMF, but achieving less emitted power.

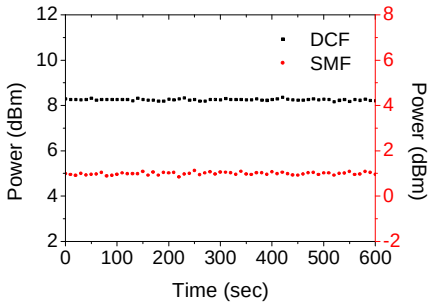

Fig. 4. Power stability evolution obtained with both fibers (DCF and SMF)

The two first system characterizations depicted in figure 3 and figure 4 consisted of, on the one hand, the lasing power evolution versus the Raman pump power and, on the other hand, the power stability along time. Both figures include the results obtained for the DCF and the SMF. These results were obtained for the highest peak power of 23 emission lines with a 100 GHz separation and without any equalization, (figure 7 (a) and figure 8 (a)). As figure 3 shows, the lasing threshold in the DCF laser occurs when the Raman pump power is 200 mW lower than in the SMF laser. This behavior is caused by the DCF fiber non-linearities, that are higher than in the SMF, being Raman amplification effect more efficient when DCF fiber is used. Anyway, as it will be explained next, the selected pump power for operation was 1.6 W in both cases.

Figure 4 shows the measured output power instability for both fibers that are lower than 0.2 dB which fits with the typical high stability Raman fiber lasers performance.

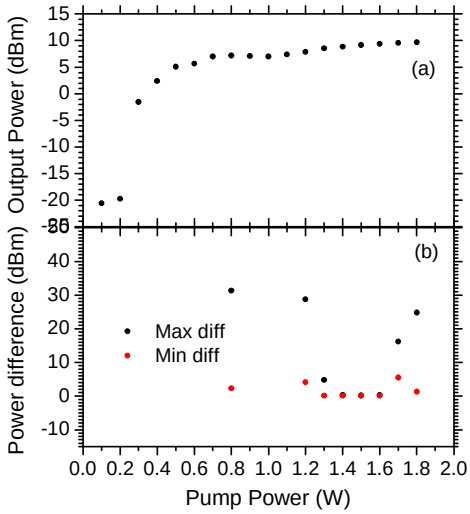

Fig. 5. Graphical demonstration of the pump power choice. The lasing power evolution vs. the pump power (a) is compared with the system stability (b), which depicts the emitted power difference for the best and worst cases.

In order to justify the 1.6 W pump power used for the measurements, in figure 5 (a) the evolution of the stability of the output power against the Raman pump is depicted. The minimum power instability is located around 1.5 W. Although

This article has been accepted for publication in a future issue of this journal, but has not been fully edited. Content may change prior to final publication. Citation information: DOI 10.1109/JLT.2015.2397191, Journal of Lightwave Technology

the system efficiency in that point is lower than when the Raman pump power is 0.6 W, the stability is higher. Figure 5 (b) shows the power difference between emission lines for the maximum difference and minimum difference. Hence, when no power difference between peaks is observed, the maximum system instability is reached. The instabilities at low Raman pump powers are due to gain competition between emission lines because the EDFA gain stands out.

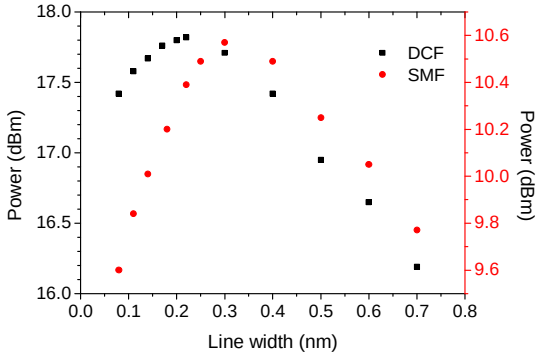

Fig. 6. One emission line output power evolution when the line width is varied.

One important parameter to consider in the design of a fiber laser with long fiber spools is its line width. As it was studied before in [15], the laser performance is proportional to its line width. This is because the generation of Brillouin scattering and other nonlinear effects, which cause that the narrower the line is, the higher line depletion occurs when it propagates along the fiber. On the other hand, the broader the line is, the less efficient the amplification is. Therefore, using the developed software, the maximum power value of one emission line was tracked while the line width was varied in a controlled way. Figure 6 shows the results obtained for the DCF and SMF spools. For a fixed pump power, an optimum line width can be empirically obtained for achieving a maximum emitted peak power. For the DCF an optimal value of ~0.2 nm width was obtained. For the SMF study, the optimal value is broader, about 0.25 nm. Notwithstanding, in a multi-wavelength laser we have to take care of more factors: stability, pump power needed and maximum number of emission lines. Finally, the optimum line widths selected were 0.24 nm for the DCF setup and 0.17 nm for the SMF one. These values offer the best performance to maximize the number of emission lines having good line output power stability.

The developed MWFL control software includes a feature to equalize the power of the emission lines. The equalization procedure of the emission lines is a key performance of the system because the equalization defines the whole spectral behavior, enhancing the number of emission lines and, of course, the flatter multi-wavelength shape. In this way, the software equalizes the lines by comparing the power difference between all the lines with the lowest one. Then, a proportional attenuation is applied to each one until the power difference fulfils a value set by the user. This proportional factor is another value to be taken under consideration. It is important that the software does not induce unjustified loss into the cavity. This factor imposes the equalization accuracy.

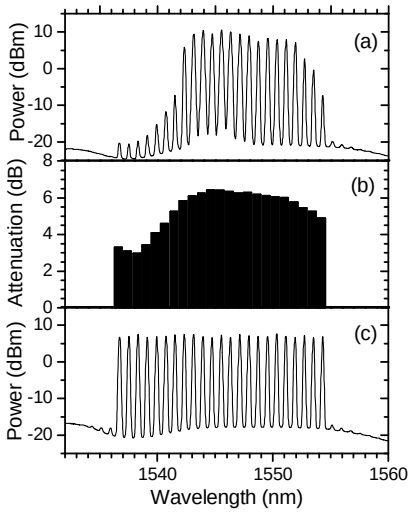

Fig. 7. Maximum number of emission lines for the DCF without equalization and the attenuation profile to equalize the spectrum with the result illustrated below.

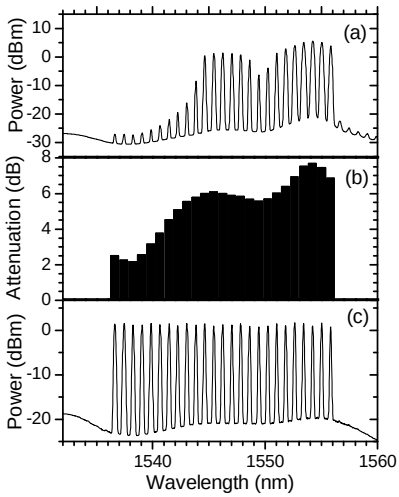

Fig. 8. Maximum number of emission lines for the SMF without equalization and the attenuation profile to equalize the spectrum with the result illustrated below.

In figures 7 and 8 the equalization process is illustrated for the 100 GHz ITU grid specification for the two fibers. First row of both plots (Fig. 7 (a) and 8 (a)) depicts the maximum number of emission lines when they are not equalized. In the second row (Fig. 7 (b) and 8 (b)), the attenuation profiles previously calculated are shown, giving way to the third row (Fig. 7 (c) and 8 (c)) which is the maximum number of emission lines for the two fibers already equalized. When the attenuation profiles are analyzed, the first bar of the attenuation profile refers to the attenuation of the lowest line depicted in figures 7 (a) and 8 (a); which in both cases are close to 0. When the equalization starts, the amplification efficiency improves the power of this line and fulfills the

This article has been accepted for publication in a future issue of this journal, but has not been fully edited. Content may change prior to final publication. Citation information: DOI 10.1109/JLT.2015.2397191, Journal of Lightwave Technology

lasing condition unlike the previous non equalized result. The equalization process continues until the power difference, as was aforementioned, is lower than the threshold set by the user, in this case 0.5 dB. We have to remark that the threshold should not be fixed at a lower value than the system worst instability.

III. Experimental Results

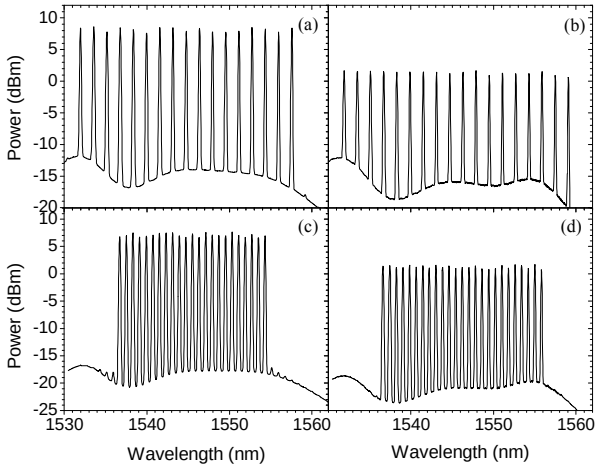

Fig. 9. Maximum number of emission lines for the 200 and 100 GHz ITU grid measured for the DCF (a and c) and the SMF (b and d).

Figure 9 depicts the maximum number of emission lines for 200 and 100 GHz wavelength spacing for the two different distributed mirrors (DCF (a-c) and SMF (b-d)). The two main differences illustrated in this figure are the number of emission lines and the output power. While DCF fiber present more output power than the SMF, this last present few more emission lines.

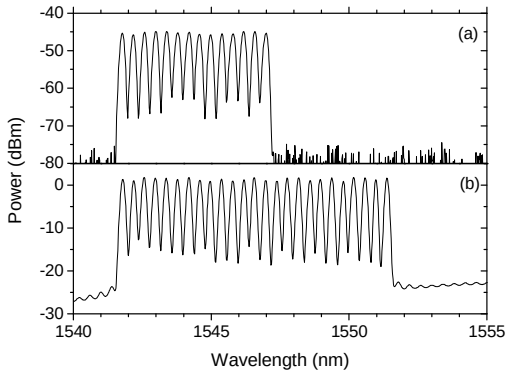

Fig. 10. Maximum number of emission lines for the 50 GHz ITU grid measured for the DCF (a) and the SMF (b).

For the 50 GHz wavelength spacing, that is the more tough case, figure 10 depicts the maximum number of emission lines for the two different distributed mirrors (DCF (a) and SMF (b)). There is some difference in the number of emission lines achieved using both fibers. This spacing causes a higher difference between both configurations. There is a difference of 11 peaks between the SMF and the DCF lasers. This can be attributable to different gain spectra and non-linear behavior presented in both fibers. DCF fiber with a smaller effective area concentrates all the amplification and higher non linear effects [16] in 2.5 km of fiber unlike the SMF, which distributes these effects along 50 km of fiber to achieve a similar gain.

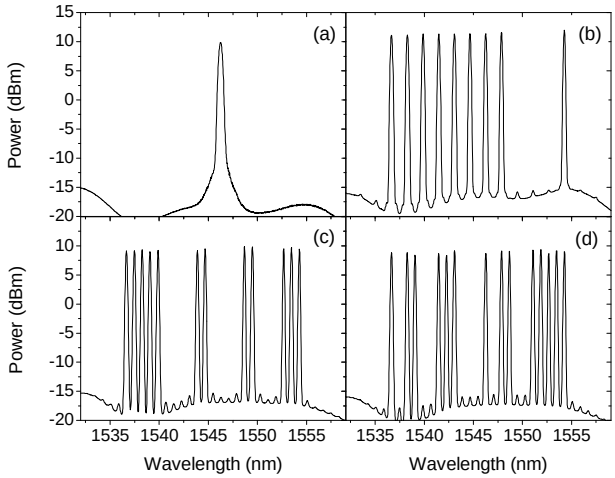

Fig. 11. Different emission lines configurations measured in B. Single wavelength (a), 9 wavelengths (b), 11 wavelengths (c), 14 wavelengths (d).

The last characteristic to be studied is the switching capability of the lasers´ spectra. Figure 11 shows different configurations of the filter already equalized when the distributed mirror was illuminated with 1.6 W Raman pump power. Figure 11 also illustrates the reconfigurability of the proposed system showing different emission patterns of lines already equalized.

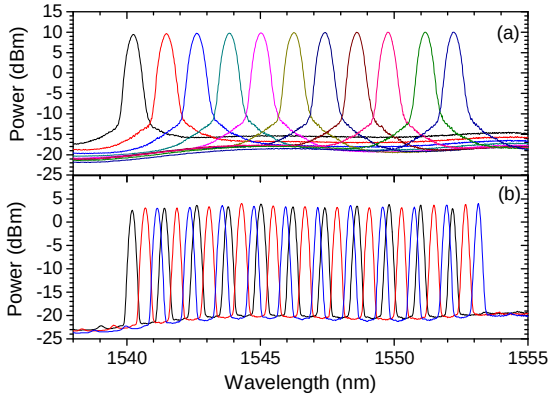

Fig. 12. MWFL configuration for single discrete wavelength sweep (a) and discrete multi-wavelength sweep (b).

Other reconfiguration skill is the discrete wavelength sweep. Thus, the programmable filter allows a maximum discrete wavelength sweep resolution of 8 pm. In figure 12 two ways to make a discrete wavelength sweep with the presented system are shown. A single discrete wavelength sweep (a) and a new technique only possible with the presented system to reduce the sweep steps and the sweeping time (b). It is the discrete multi-wavelength sweep. Once fixed the wavelength range to be scanned, the MWFL sweeps the spectrum spending a lower number of sweep steps. Thus, the number of steps is inversely proportional to the number of

This article has been accepted for publication in a future issue of this journal, but has not been fully edited. Content may change prior to final publication. Citation information: DOI 10.1109/JLT.2015.2397191, Journal of Lightwave Technology

emission lines chosen. For example, while a single wavelength sweep need twenty cycles to sweep a band, a five lines multi-wavelength laser sweep only needs four.

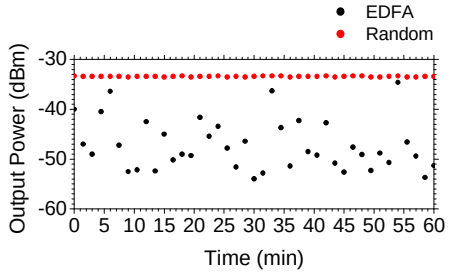

Fig. 13. Output power variations of the multi-wavelength random laser in comparison with a non-distributed (EDFA based) laser cavity.

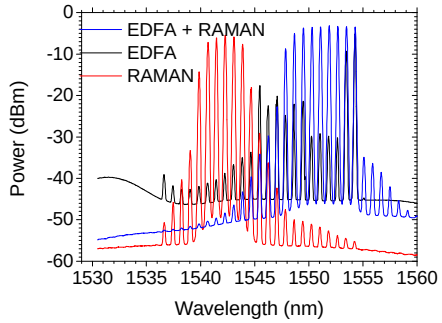

Fig. 14. Comparison of different spectra when different amplification media were used.

Finally, in order to justify the use of the EDFA and RDFB amplification, in figure 13 it is shown a comparison of the stability for the distributed mirror based cavity and an EDFA based linear cavity. For this study, a 30 emission lines configuration for a 100 GHz grid was selected. In figure 13 it is demonstrated the high stability of the laser when the distributed mirror is used; unlike the high instabilities achieved with the non random configuration. Gain competition between emission lines affects mainly this last case, as expected because of the different nature of the amplification media [17]. Therefore, the use of the Raman based distributed mirror is crucial, making this structure stable. In addition, when the amplification process is complemented with EDFA gain, a broader result is obtained. Figure 14 shows the comparison of the laser cavity spectra when different amplification media are used. This figure also demonstrates the importance of the combination of both amplification methods to achieve a more stable and broader result.

IV. Proof of Concept Sensor Network

Figure 15 shows a remote multiplexing sensor network that was used to demonstrate the advantages of the aforementioned switchable multi-wavelength fiber laser. This network is connected by the WDM to the MWFL at point B depicted in figure 1. We have proposed two different sensors networks which are based on completely different operation modes. A multiplexing network of 7 high birefringence photonic crystal fiber (HiBi PCF) intensity based strain sensors [8] and a 11 FBG wavelength based temperature/strain sensors array.

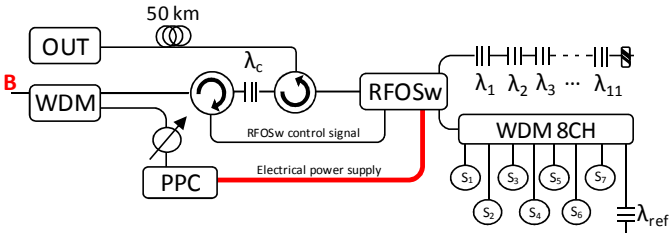

Fig. 15. Proof of concept remote sensor network schematic setup.

The sensors network's performance is as follows. On the one hand, the residual Raman pump is collected at point B from the distributed mirror by the 1445 port of a 1445/1550 WDM. This Raman pump excess is used to feed a remote powered by light fiber optic switch (RFOSw), previously reported in [18]. The RFOSw converts 125 mW of the residual Raman pump of the distributed mirror onto 35 mW of electrical power using a photovoltaic power converter (PCC) PCC9LW made by JDSU.

On the other hand, the laser signal is launched through the 1550 port (B). Firstly, the control signal, only in the PCF sensors case, is filtered and redirected to the RFOSw by the first circulator and a FBG centered at its wavelength (λ_c). The second circulator has the objective of illuminating the RFOSw and collecting the sensors networks information. This information is launched towards the system output port placed after 50 km fiber at the signal header. Finally, the RFOSw selects alternatively both sensors networks depending on the channel selection signal, labeled as "RFOSw control signal" in figure 15. Therefore, when the signal is ON, the HiBi PCF sensor network is selected. When the control signal is OFF, the FBG sensors array is interrogated.

A- HiBi PCF sensors network

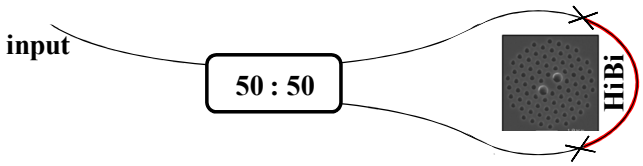

Fig. 16. HiBi PCF sensor schematic diagram and a HiBi PCF section's picture.

The HiBi PCF sensor network consists of 7 PCF strain sensors. These sensors are formed of ~1.5 m of HiBi PCF (PM-1550-01 from NKT Photonics) connected into a Sagnac loop mirror structure as depicted in figure 16. When the fiber is strained the achieved inter-polarization-modes interference shifts in wavelength. Thus, when a fixed wavelength illuminates the structure, it is reflected and its intensity is modulated proportionally to the interference position corresponding to the applied strain. Therefore, the 7 PCF-based sensors are connected to an 8 channel WDM (from 1536.61 to 1547.72 in 200 GHz ITU grid spec.) and the free channel was connected to a FBG which acts as sensor´s reference. The laser spectrum used to interrogate this network was depicted in figure 11 (b).

This article has been accepted for publication in a future issue of this journal, but has not been fully edited. Content may change prior to final publication. Citation information: DOI 10.1109/JLT.2015.2397191, Journal of Lightwave Technology

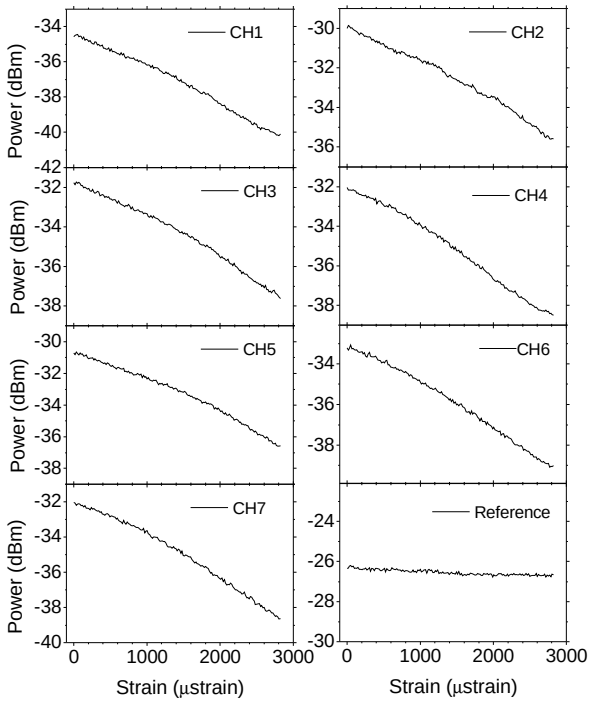

Fig. 17. 7 HiBi PCF strain sensors power evolution vs. strain and reference channel's FBG reflection.

Figure 17 depicts the 7 sensors strain's characterization and the reference arm response. 10 cm of the sensing fiber were glued into a motorized high precision translation stage which strained the fiber 0.017 mstrain per step. Studying previous results, the proposed sensors present a strain sensitivity of ~2.23 dBm/mstrain with a measurement uncertainty of 0.09 mstrain. Furthermore, due to the multiplexing structure performed, this sensor network is crosstalk free as figure 18 demonstrates. In this figure, results when CH6 sensor is stressed and when CH1 sensor is not stressed are shown.

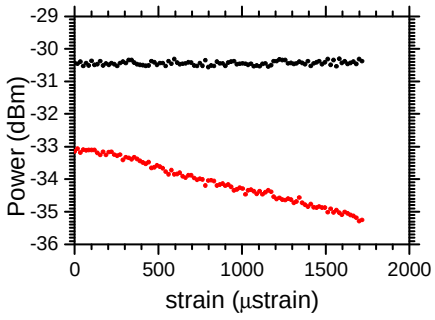

Fig. 18. System's crosstalk free demonstration. It is illustrated the CH6 strain sensor result in red and CH1 sensor response while it is not stressed.

B- 11 FBG sensors array.

When the control signal is OFF, FBG sensors channel is selected. In this mode, the laser structure works as a discrete wavelength sweep laser with a resolution of 0.01 nm. Figure 13 (a) illustrates only the 11 emission lines, which correspond with the 11 FBG, of the 1500 emission lines needed to scan the entire FBG network. Thus, figure 19 depicts the reconstruction of the 11 FBG reflections when the discrete wavelength sweep emission line fit each FBG maximum.

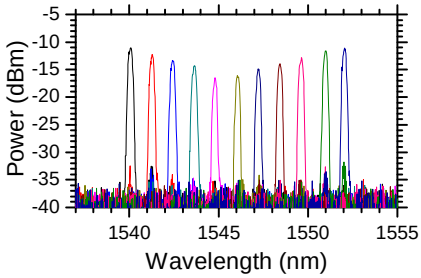

Fig. 19. Spectral composition of the FBG sensors network interrogation result.

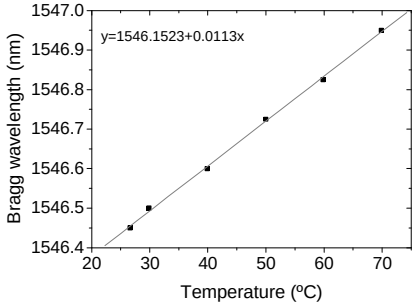

Fig. 20. Temperature response of the 1546.4 nm FBG sensor.

Finally, figure 20 shows the 1546.4 nm FBG temperature's characterization in order to demonstrate the correct FBG sensors network performance. This plot illustrates the maximum wavelength achieved for the different temperatures. It shows the usual ~0.01 nm/ºC FBG thermal sensitivity. Hence, a temperature resolution of 1 ºC is obtained.

V. Conclusions

An in real-time switchable and reconfigurable multi-wavelength fiber laser has been experimentally demonstrated. It has been characterized using two fibers, 2.5 km of DCF and 50 km SMF. This laser shows high stability, a broad-band response, reconfigurability, versatility and high power emission lines. A maximum band of ~20 nm can be reconfigured with a minimum distance of 50 GHz between lasing channels. However, the best performance of the laser is achieved when the emission lines distance is 100 GHz. This structure can be equalized and switched fulfilling the 50 GHz ITU grid specification when the SMF is used. It has been also demonstrated that by equalizing the spectra, more emission lines than without equalization are achieved.

Two multiplexing sensors networks were simultaneously interrogated by using a remote powered by light fiber optic switch and the developed laser. The Raman pump excess of the random mirror structure is used to feed the RFOSw. This technique can multiplex as sensors networks as output ports the switch have. Furthermore, as the control signal is generated by the fully switchable MWFL, the laser spectrum change also entails the RFOSw port selection. Therefore, this MWFL proposal seems to fit perfectly with optical communications applications as well as for fiber optic sensors multiplexing, as it was demonstrated in this paper.

This article has been accepted for publication in a future issue of this journal, but has not been fully edited. Content may change prior to final publication. Citation information: DOI 10.1109/JLT.2015.2397191, Journal of Lightwave Technology

REFERENCES

[1] S. K. Turitsyn, S. A. Babin, A. E. El-Taher, P. Harper, D. V. Churkin, S. I. Kablukov, J. D. Ania-Castañon, V. Karalekas, and E. V. Podivilov, "Random distributed feedback fibre laser", Nature Photonics, vol. 4, 2010.

[2] A. E. El-Taher, M. Alcon-Camas, S. A. Babin, P. Harper, J. D. Ania-Castañón, and S. K. Turitsyn, "Dual-wavelength ultralong Raman laser with Rayleigh-scattering feedback", Optics Letters, vol. 35, pp. 1100-1102, 2010.

[3] M. Fernandez-Vallejo, M. Bravo, M. Lopez-Amo, "Ultra-Long Laser Systems for Remote Fiber Bragg Gratings Arrays Interrogation," Photonics Technology Letters, IEEE , vol. 25, pp. 1362-1364, 201.)

[4] A. M. R. Pinto, O. Frazão, J. Santos, M. Lopez-Amo, "Multiwavelength fiber laser based on a photonic crystal fiber loop mirror with cooperative Rayleigh scattering", Appl. Phys. B, vol. 99, pp. 391–395, 2010.

[5] A. M. R. Pinto, M. Lopez-Amo, "Double random mirror Hi–Bi photonic crystal fiber Sagnac based multiwavelength fiber laser", Appl. Phys. B vol. 103, pp 771–775, 2011.

[6] A. M. R. Pinto, O. Frazão, J. L. Santos, and M. Lopez-Amo, "Multiwavelength Raman Fiber Lasers Using Hi-Bi Photonic Crystal Fiber Loop Mirrors Combined With Random Cavities", Journal of Lightwave Technology, vol. 29, 2011.

[7] V. DeMiguel-Soto, M. Bravo and M. Lopez-Amo, "Fully-switchable multi-wavelength fiberlaser assisted by a Random mirror", Optics Letters, Vol. 39, pp. 2020-2023, 2014.

[8] A. M. R. Pinto, M. Bravo, M. Fernandez-Vallejo, M. Lopez-Amo, J. Kobelke and K. Schuster "Suspended-core fiber Sagnac combined dual-random mirror Raman fiber laser", Optics Express, Vol. 19, pp. 11906-11915, 2011.

[9] A. E. El-Taher, P. Harper, B. Babin, D. Churkin, E. Podivilov, J. D. Ania–Castañon, S.K. Turitsyn, "Effect of Rayleigh-scattering distributed feedback on multiwavelength Raman fiber laser generation", Optics Lett vol. 36, pp. 130-132, 2011.

[10] S. Sugavanam, Z. Yan, V. Kamynin, A. S. Kurkov, L. Zhang, D. V. Churkin, "Multiwavelength generation in a random distributed feedback fiber laser using an all fiber Lyot filter", Opt. Express, vol. 22, pp. 2839–2844, 2014.

[11] S. K. Turitsyn, S. A. Babin, D. V. Churkin, I. D. Vatnik, M. Nikulin, and E. V. Podivilov, "Random distributed feedback fiber lasers", Physics Reports., vol. 542, pp. 133-193, 2014.

[12] Perez-Herrera, R. A., Fernandez-Vallejo, M., Diaz, S., Quintela, M. A., Lopez-Amo, M., and Lopez-Higuera, J. M., "Stability comparison of two quadruple-wavelength switchable erbium-doped fiber lasers", Optical Fiber Tech., vol. 16, 2010.

[13] Rota-Rodrigo, S., Rodriguez-Cobo, L., Quintela, M. A., Lopez-Higuera, J. M., and Lopez-Amo, M., "Switchable fiber optic laser system for high and low-strain fiber optic sensors remote multiplexing", Proc. SPIE 5th EWOFS, 8794-47, 2013.

[14] M. Bravo, V. DeMiguel-Soto, A. Ortigosa and M. Lopez-Amo, "Fully switchable multi-wavelength fiber laser based interrogator system for remote and versatile fiber optic sensors multiplexing structures" Proc. SPIE, 23rd OFS conference, 9157, 91576P, 2014.

[15] M. Fernandez-Vallejo, S. Rota-Rodriguez, and M. Lopez-Amo, "Remote (250 Km) fiber Bragg grating multiplexing system" Sensors, vol. 11, pp. 8711-8720, 2011.

[16] A. R. Chraplyvy, "Limitations on Lightwave Communications Imposed by Optical-Fiber Nonlinearities", Journal of Lightwave Technology, vol. 8, pp. 1548-1557, 1990.

[17] M. Fernandez-Vallejo, S. Diaz, R. A. Perez-Herrera, R. Unzu, M. A. Quintela, J. M. Lopez-Higuera and M. Lopez-Amo M, "Comparison of the Stability of Ring Resonator Structures for Multiwavelength Fiber Lasers Using Raman or Er-Doped Fiber Amplification" IEEE J. Of Quantum Electronics, vol. 45, pp.1551-1556, 2009.

[18] M. Bravo, M. A. Erro, J. M. Algueta, S. Diaz and M. Lopez-Amo, "Remote fiber optic switch powered by light for robust interrogation of fiber Bragg grating sensor networks", Measurement Science and Technology, vol. 24, 2013.